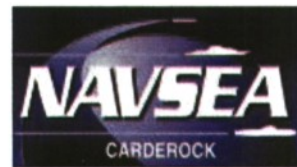


Carderock Division  
**Naval Surface Warfare Center**  
West Bethesda, Maryland 20817-5700



NSWCCD-50-TR-2009 / 010 December 2009  
Hydromechanics Department Report

**Joint High Speed Sealift (JHSS) Appendage Resistance  
Computational Fluid Dynamics (CFD) Analysis**

by  
Minyee Jiang



Approved for Public Release: Distribution Unlimited

**20100225015**

# REPORT DOCUMENTATION PAGE

*Form Approved*  
*OMB No. 0704-0188*

Public reporting burden for this collection of information is estimated to average 1 hour per response, including the time for reviewing instructions, searching existing data sources, gathering and maintaining the data needed, and completing and reviewing this collection of information. Send comments regarding this burden estimate or any other aspect of this collection of information, including suggestions for reducing this burden to Department of Defense, Washington Headquarters Services, Directorate for Information Operations and Reports (0704-0188), 1215 Jefferson Davis Highway, Suite 1204, Arlington, VA 22202-4302. Respondents should be aware that notwithstanding any other provision of law, no person shall be subject to any penalty for failing to comply with a collection of information if it does not display a currently valid OMB control number. **PLEASE DO NOT RETURN YOUR FORM TO THE ABOVE ADDRESS.**

<b>1. REPORT DATE (DD-MM-YYYY)</b> 12-31-2009			<b>2. REPORT TYPE</b> Final			<b>3. DATES COVERED (From - To)</b> March 2007 to Oct. 2008			
<b>4. TITLE AND SUBTITLE</b> Joint High Speed Sealift (JHSS) Appendage Resistance Computational Fluid Dynamics (CFD) Analysis						<b>5a. CONTRACT NUMBER</b>			
						<b>5b. GRANT NUMBER</b>			
						<b>5c. PROGRAM ELEMENT NUMBER</b>			
<b>6. AUTHOR(S)</b> Minyee Jiang						<b>5d. PROJECT NUMBER</b>			
						<b>5e. TASK NUMBER</b>			
						<b>5f. WORK UNIT NUMBER</b>			
<b>7. PERFORMING ORGANIZATION NAME(S) AND ADDRESS(ES) AND ADDRESS(ES)</b>  Naval Surface Warfare Center Carderock Division 9500 Macarthur Boulevard West Bethesda, MD 20817-5700						<b>8. PERFORMING ORGANIZATION REPORT NUMBER</b>  NSWCCD-50-TR-2009/010			
<b>9. SPONSORING / MONITORING AGENCY NAME(S) AND ADDRESS(ES)</b> Mr. Steve Wynn (NAVSEA 05D1) Naval Sea System Command 1333 Isaac Hull Ave., SE Washington, DC 20376-5061						<b>10. SPONSOR/MONITOR'S ACRONYM(S)</b>			
						<b>11. SPONSOR/MONITOR'S REPORT NUMBER(S)</b>			
<b>12. DISTRIBUTION / AVAILABILITY STATEMENT</b>  Approved for Public Release; Distribution Unlimited									
<b>13. SUPPLEMENTARY NOTES</b>									
<b>14. ABSTRACT</b>  The appendage drag of the surface ship, Joint High Speed Sealift (JHSS), has been estimated by various empirical methods with drag coefficients for the separate appendage components. These empirical methods have been shown to be inaccurate when the interaction between appendage components is considered. Recently, several existing methodologies for the existing appendage drag were reviewed. In this study, Computational Fluid Dynamics (CFD) using the Reynolds Averaged Navier-Stokes (RANS) equations was chosen to perform drag analysis on several configurations with different turbulence models. A breakdown resistance contribution list for all the appendage elements is also provided in this study.									
<b>15. SUBJECT TERMS</b> JHSS, CFD, Appendage, Resistance									
<b>16. SECURITY CLASSIFICATION OF:</b>						<b>17. LIMITATION OF ABSTRACT</b>  SAR	<b>18. NUMBER OF PAGES</b>  21	<b>19a. NAME OF RESPONSIBLE PERSON</b> Minyee Jiang	
<b>a. REPORT</b> UNCLASSIFIED	<b>b. ABSTRACT</b> UNCLASSIFIED	<b>c. THIS PAGE</b> UNCLASSIFIED			<b>19b. TELEPHONE NUMBER</b> (301) 227-6090				

THIS PAGE INTENTIONALLY LEFT BLANK

## Contents

	Page
Abstract.....	1
Administrative Information .....	1
Introduction.....	1
Geometry.....	2
Configurations for CFD Model and Run Matrix .....	4
Grid Generation .....	5
Boundary and Flow Conditions .....	7
CFD Solution Analysis .....	8
Total Drag Comparison.....	8
The Effect of Propeller Hub and Fairwater.....	10
The Detail Break Down of Drag Contribution from Each Element .....	14
Conclusions.....	17
References.....	19

## Figures

	Page
1. JHSS BSS bow design variations .....	2
2. JHSS BSS FA, dry-dock photographs .....	2
3. Grid on the domain boundaries and on the hull.....	5
4. Grid distribution on the hull and appendages .....	6
5. Boundary conditions.....	7
6. Comparison of surface grid on the appendages with and without propeller extension hub fairwater.....	10
7. Comparison of the flow separation on the appendages with propeller extension hub fairwater (left) and without propeller extension hub fairwater (right).....	11
8. Comparison of pressure contours on the appendages with propeller extension hub fairwater (left) and without propeller extension hub fairwater (right).....	12
9. Comparison of pressure contours on the appendages with propeller extension hub fairwater (left) and without propeller extension hub fairwater (right) (close up view) .....	12
10. Appendage elements of inboard and outboard sets .....	14
11. Pressure contours on the inboard and outboard fairwaters.....	15

## Tables

	Page
1. JHSS: BSS, bow variations, dynamic sinkage and pitch for baseline bulb (BB) dynamic conditions; Exp5 BSS BH DES .....	3
2. JHSS: BSS, bow variations, dynamic sinkage and pitch for baseline bulb (BB) dynamic conditions; Exp2 BSS FA DES .....	3
3. Computed configurations for the JHSS baseline bulb (BB) .....	4
4. Run matrix .....	4
5. Grid size for each configuration .....	6
6. Comparison of the total drag between the measured data and the RANS calculation .....	9
7. Comparison of appendage drag with measured data and CFD predictions .....	9
8. Resistance contributions from the appendages .....	11
9. Resistance contributions from the appendages .....	13
10. RANS calculation for the appendage resistance study .....	15

## **Abstract**

*The appendage drag of the surface ship, Joint High Speed Sealift (JHSS), has been estimated by various empirical methods with drag coefficients for the separate appendage components. These empirical methods have been shown to be inaccurate when the interaction between appendage components is considered. Recently, several existing methodologies for the existing appendage drag were reviewed. In this study, Computational Fluid Dynamics (CFD) using the Reynolds Averaged Navier-Stokes (RANS) equations was chosen to perform drag analysis on several configurations with different turbulence models. A breakdown resistance contribution list for all the appendage elements is also provided in this study.*

## **Administrative Information**

The work described in this report was sponsored by the JHSS Project Office, NAVSEA 05D1, Project Manager Mr. Steven Wynn. The work was performed at the Naval Surface Warfare Center Carderock Division (NSWCCD) by the Computational Hydrodynamics Division (Code 5700) under job order number 07-1-2125-146-48.

## **Introduction**

Several existing empirical methods have been used for appendage drag predictions. However, there are several known problems when multiple appendage components are involved in the estimation. Previous attempts using typical drag coefficients and assembly of individual pieces have had difficulty related to accounting for overlapped areas and interference among pieces; using the actual flow field velocity as opposed to just ship speed; scale effects and the best drag coefficient selection.

There are many commercial numerical tools available, both empirical and numerical methods, that are capable of providing the powering prediction for ships [1~4]. Recently a separate study was performed at NSWCCD which used two appendage resistance prediction programs [5, 6], which are adapted for PC execution, and are further coded with EXCEL spreadsheet for easy parametric studies [7].

In the last decades, multiple Reynolds Averaged Navier-Stokes (RANS) Computational Fluid Dynamics (CFD) tools, both commercial and university based, have been developed and validated for maritime applications. In this study, one of the commercial solvers, CFD++, was chosen to perform drag analysis on the configurations. CFD++, developed by Metacomp Technologies, has been efficiently applied to numerous applications solving incompressible steady and unsteady flows. CFD++ allows for easy treatment of complex geometries by using unification of structured, unstructured and multi-block grids. In addition, wall-functions can be used for further reducing the grid size for a complex geometry.

Four configurations from fully appended to the bare hull have been included in this study. The CFD predictions will be used to compare with the model test data [8] and the contribution of drag on each appendage surface will be investigated in this study. The results can be utilized for design reference in the future.

## Geometry

Resistance and Propulsion Model 5653, representative of the JHSS baseline shaft and struts (BSS) hull form, was selected for this appendage drag analysis. Four bulb designs, Baseline Bulb (BB), Elliptical Bulb (EB) and a Stern Bow (ST) are included in the model test, but only the Baseline Bulb is modeled in the CFD study. A photo of the bare hull shell of Model 5653 is in Figure 1 where the baseline bulb is shown at the middle of the three bulb models. The appendages in the model test include propeller shafts, struts, barrels and rudders which are shown in Figure 2.

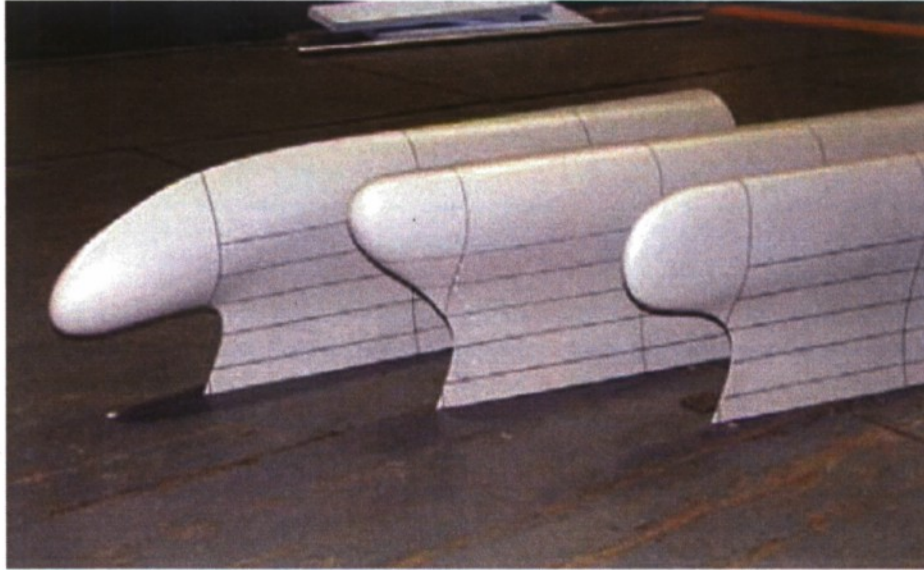


Fig. 1 JHSS BSS bow design variations

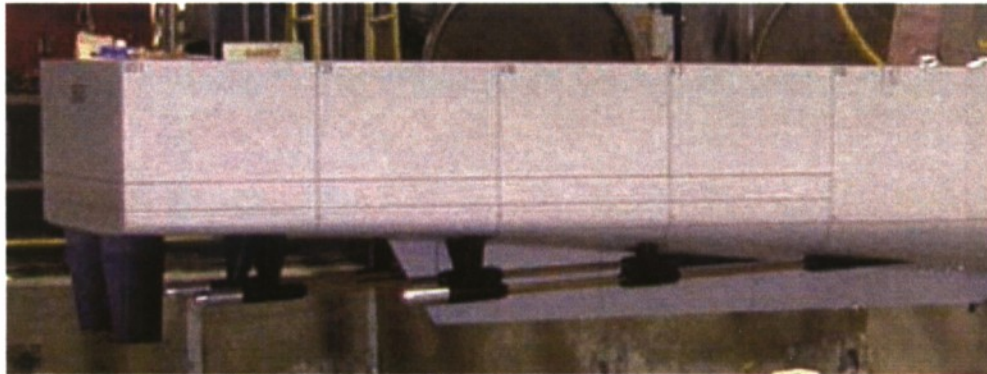


Fig. 2 JHSS BSS FA, dry-dock photographs

Based on the model test Exp 5 BSS BH DES from table B18 of reference [8], the basic sinkage and trim information for the model position and the flow speed of the bare hull configuration are listed in Table 1. Similarly, the position information of the fully appended configuration is shown in Table 2.

Table 1 JHSS: BSS, bow variations, dynamic sinkage and pitch for baseline bulb (BB) dynamic conditions; Exp5 BSS BH DES

	VS (knots)	Sinkage FP (ft)	Sinkage AP (ft)	Pitch Angle (degree)	FP Draft (ft)	AP Draft (ft)
Full Scale	36	4.27	-0.36	-0.28	33.10	28.47
Model Scale	6.16	0.1251	-0.0105	-0.28	0.970	0.834

Table 2 JHSS: BSS, bow variations, dynamic sinkage and pitch for baseline bulb (BB) dynamic conditions; Exp2 BSS FA DES

	VS (knots)	Sinkage FP (ft)	Sinkage AP (ft)	Pitch Angle (degree)	FP Draft (ft)	AP Draft (ft)
Full Scale	36	4.03	-0.05	-0.25	32.86	28.78
Model Scale	6.16	0.1181	-0.001	-0.25	0.963	0.843

Some abbreviations for Table 1 and Table 2 are defined as:

BSS        Baseline shafts and struts  
 BH        Bare hull  
 FA        Fully Appended  
 DES       Design displacement

### Configurations for CFD Model and Run Matrix

There are four configurations included in this appendage drag study which are shown in Table 3. The fully appended configuration (FA) includes ship hull, four sets of propeller shafts, four sets of struts, four barrels and two rudders. The next two configurations are stripped down from the fully appended configuration by excluding two rudders and then by excluding all the appendages. The approach of stripping down the model from the fully appended configuration provides a consistent grid quality for comparison. For example, when the rudders were removed the grid was modified only locally, without altering the grid in the global domain. In this way, the flow field in the global domain will remain similar up to the rudders. Therefore, the calculation of the resistance contribution from the rudders will be more accurate without concerns of grid inconsistency.

An additional configuration was added to study the effect of the fairwater. The propeller hub has been added to the last shaft barrel and a fairwater was added to the barrel to form smoother contours to the end the shaft. This small geometry extension significantly reduces flow separation at the end of the second shaft barrel, which should be carefully counted in the measurement for resistance prediction.

Table 3 Computed configurations for the JHSS baseline bulb (BB)

Configurations	Description
FA	Model 5653 hull + propeller shafts + struts + barrels + rudders
FA -Rudder	Model 5653 hull + propeller shafts + struts + barrels
FA – Appendage (bare hull)	Model 5653 hull
FA + propeller hub and fairwater	Model 5653 hull + propeller shafts + struts + barrels + rudders + fairwater

Two turbulence models, Realizable k- $\epsilon$  [Ref 9,10] and k- $\epsilon$ -Rt [Ref 11,12] have been added to the variation of configurations and form a calculation matrix for the appendage resistance study for JHSS, which is shown in Table 4.

Table 4 Run matrix

Cases #	Configuration	Turbulence model
1	Fully Appended Configuration (FA)	k- $\epsilon$ -Rt
2	FA + propeller hub & fairwater	k- $\epsilon$ -Rt
3	FA – rudder	k- $\epsilon$ -Rt
4	FA- Appendages (Bare Hull)	k- $\epsilon$ -Rt
5	Fully Appended Configuration (FA)	Realizable k- $\epsilon$
6	FA + propeller hub & fairwater	Realizable k- $\epsilon$
7	FA – rudder	Realizable k- $\epsilon$
8	FA- Appendages (Bare Hull)	Realizable k- $\epsilon$

## Grid Generation

Unstructured grid topology is a practical method to generate grids for complex geometries. It is especially useful in dealing with multiple elements in close proximity. The unstructured topology allows a user to concentrate on building a surface grid on each element without concern over matching cell numbers on the nearby elements. This grid topology provides great freedom in distributing grid cells to the most needed areas. The grid generation tool, Gridgen, which is developed by Pointwise, was used to generate all the grids for this study. Although Gridgen is capable of constructing structured, unstructured or hybrid grids, only an unstructured grid topology was used in this study.

In the process of grid generation for this model, first of all, the geometry has to be carefully examined and all the gaps and holes in the geometry should be repaired before it is ready for the grid generation tool. The tool for geometry repair and preparation is Rhinoceros. Second, using Gridgen, the given geometry was triangulated to form surface grid cells on the hull and appendages. In order to accurately simulate the flow, grid points were clustered in areas where high velocity gradients are expected, which are around the bow dome and stern appendages in this model. Third, the surface grid was extruded outward from the wall boundaries to form the prism layers which are needed for capturing the detail boundary layer flow near the walls. In the final grid there are 29 prism layers used in the near wall regions. Finally, after the prism layers are formed, the rest of the domain was filled with tetrahedral cells. A sample of the unstructured grid for the fully appended configuration is shown in Figure 3.

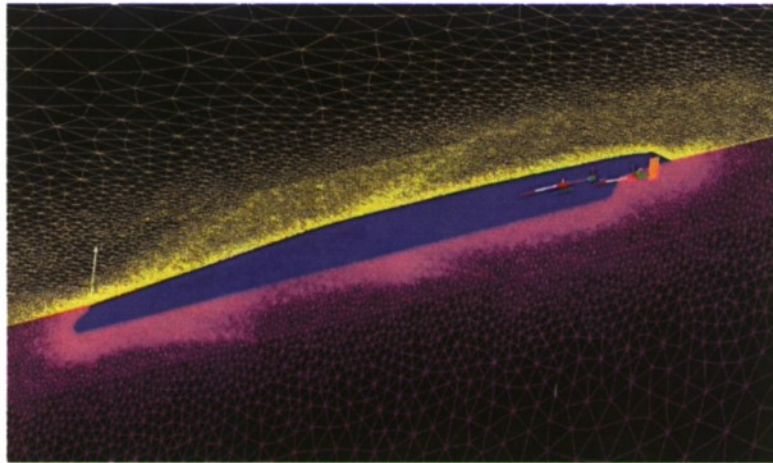


Fig. 3 Grid on the domain boundaries and on the hull

In order to maximize the number of grid cells used in this study two assumptions have been applied to this grid, which leads to more efficient use of the computer resource. Since the focus of this project is to find the contribution of the appendage drag, the free surface calculation can be eliminated by applying the double hull assumption. The concept of the double hull method is to symmetrically place a reversed hull in the vertical direction to form an imaginary domain. Therefore, the free surface effect is neglected in the process. The top surface indicated in yellow in Figure 3 is the symmetric plane between the computational domain and the imaginary domain. This symmetric plane, which will remain

as a flat surface during the calculation, can be treated as a rigid boundary. A close up view of the stern appendages is shown in Figure 4.

Furthermore, the ship is symmetric for the starboard and port such that the computational domain can be further reduced to one side where the port side was chosen in this study. The magenta surface in Figure 3 represents this symmetry boundary between starboard and port. The total number of grid cells can be significantly reduced by using the combination of the symmetry boundary and double hulls method. One can then cluster grid cells in the stern region and on the appendage surfaces for better capturing the detail of the flow features.

The computational grids for various configurations used for the RANS calculations are listed in Table 5. There are four configurations in this study and the nomenclature of these configurations has been described in the previous section. In order to capture the detailed flow field between the appendage and the hull the fully appended configuration required 9.15 million cells where a significant amount of grid cells were used in the stern region. Approximately one million grid cells were eliminated by removing the rudder from the fully appended configuration in configuration 2. In the third configuration for the bare hull only 2.3 million cells were used. Finally, in configuration 4, fully appended with propeller hub and fairwater, the total cell count increased slightly from the fully appended configuration.

Table 5 Grid size for each configuration

Configuration	Description	Number of cells (million)
1	FA (fully appended)	9.15
2	FA – rudders	8.18
3	FA – appendages	2.30
4	FA + propeller hub and fairwater	9.30

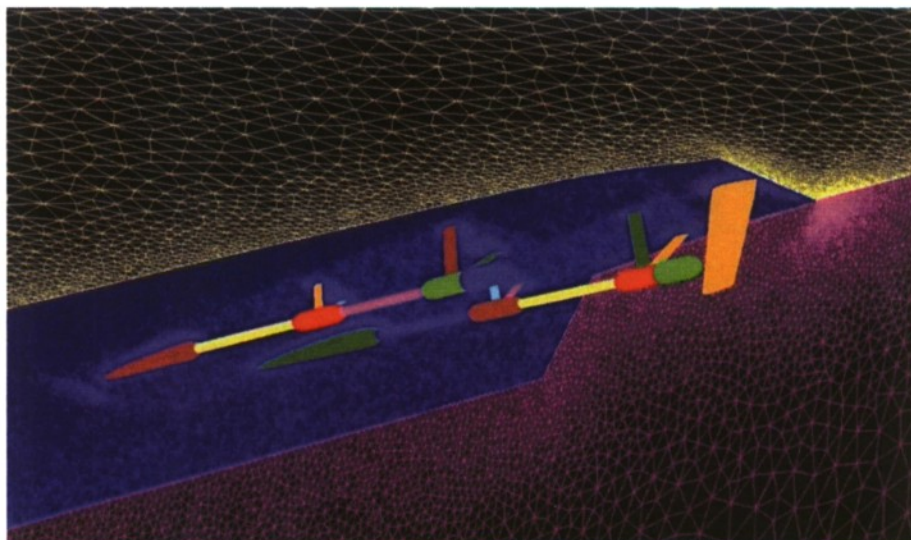


Fig. 4 Grid distribution on the hull and appendages

## Boundary and Flow Conditions

The boundary conditions for the computational model are shown in Figure 5, where the two blocks are identical. The block at the left is shown solid and the block at the right is shown transparently, which allows us to view the boundaries at the back side of the block.

The purple face on the top of the model is the rigid boundary from the double hull method, which was defined as a slip wall. The blue face is the symmetric boundary for geometry symmetry. The outlet boundary, which can be identified as magenta, is located at the far right side in the transparent block in Figure 5. The inlet velocity was specified as 6.16 knots, at model scale, which is equivalent to 36 knots at full scale. The red face is the pressure outlet and the orange face in the transparent block on the right side of Figure 5 indicates the velocity inlet. The rest of the boundaries at the bottom and the opposite side of the blue face are far field conditions.

The computational domain is two ship lengths from bow to the inlet; three ship lengths in the downstream direction; one and one-half ship length beneath the hull and three ship lengths away from the hull in the port direction.

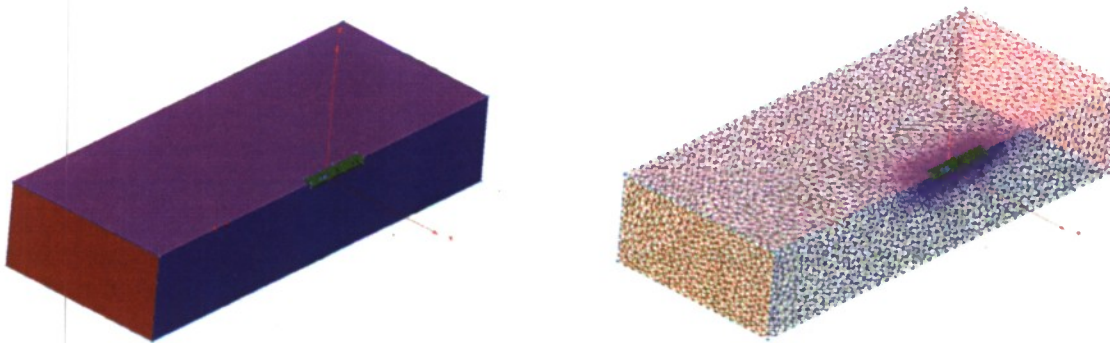


Fig. 5 Boundary Conditions

## CFD Solution Analysis

Predicting the resistance force and detailed flow field about the surface ship involves solving the Navier-Stokes equations. The most practical method today for solving the Navier-Stokes equations is the Reynolds average Navier-Stokes (RANS) method. The RANS method accounts for the effect of turbulence by involving additional equations which model the Reynolds stress terms in the Navier-Stokes equations. Numerous models have been developed and applied to different applications. For incompressible flow, the  $k$ - $\epsilon$  model, a two-equation turbulence model, has been widely used and has proved effective in predicting simple wall bounded shear flows. Here two additional equations, the turbulent kinetic energy,  $k$ , and the turbulent kinetic energy dissipation rate,  $\epsilon$ , are used to model turbulence in the Navier-Stokes equations. However, in some cases the traditional  $k$ - $\epsilon$  model does not adequately predict separated flow with an adverse pressure gradient in wall-bounded flows.

Consequently, two improved methods for modeling turbulence were also used in this study. One method is the realizable  $k$ - $\epsilon$  model, developed by Shih [9], which includes a new formulation for the turbulent viscosity and a new transport equation for the dissipation rate. The realizable  $k$ - $\epsilon$  model has been widely used in recent years and indicates good agreement with other  $k$ - $\epsilon$  model predictions [10] where appropriate. The second improved method, the  $k$ - $\epsilon$  Rt method, originally developed by Goldberg [11], carries an additional equation for the undamped eddy viscosity,  $R$ , which is independent of the  $k$  and  $\epsilon$  equations. The  $k^2/R$  term has been used to replace the dissipation rate,  $\epsilon$ , as the dissipation term in the  $k$  equation. This leads to a lowering of the turbulence level in recirculation zones enabling improved prediction of such regions [12]. Originally the  $k$ - $\epsilon$  Rt method in CFD++ was developed to resolve compressible wall bounded flow and it has been proven to do better than the standard  $k$ - $\epsilon$  model in solving separated flow regions. Both the standard realizable  $k$ - $\epsilon$  model and the  $k$ - $\epsilon$  Rt model are used in this study. The comparison will be discussed in the following sections.

## Total Drag Comparison

The comparison of the total resistance between the measured data and the CFD calculations is provided in Table 6. There are three configurations in this comparison, the fully appended (FA), the fully appended less rudders, and the bare hull. The second column in Table 6 shows the measured total drag in pound force for each configuration. The third and fourth columns show the CFD predicted total resistance with  $k$ - $\epsilon$  Rt and realizable  $k$ - $\epsilon$  turbulence models. The difference between the measured data and CFD prediction with the same configuration divided by the measured data forms the deviation percentages which are shown in the brackets. Based on this comparison, the  $k$ - $\epsilon$  Rt model over predicted the resistance of the fully appended configuration by 6.7%, it also over predicted resistance for the fully appended without rudders by 5.9%. But the  $k$ - $\epsilon$  Rt model under predicted the bare hull drag by 2.6%. In comparison, the realizable  $k$ - $\epsilon$  model under predicted all the configurations by 2.6% to 6.1%. The CFD model in this study used the double hull approach, which forms no hull wave. Typically the hull wave contributes additional drag to total ship resistance. Therefore the total resistance from a CFD prediction with the double hull approach should be less than the measured data. Since the realizable  $k$ - $\epsilon$  model predicted less total drag than the measured data, its prediction is consistent with the fact that surface waves are not part of the simulation.

Table 6 Comparison of the total resistance between the measured data and the RANS calculation

description	Fx (measured)	Fx (Computation) lbf	Fx (Computation) lbf
	lbf	[Deviation (%)]	[Deviation (%)]
		<i>k-ε</i> Rt	Realizable <i>k-ε</i>
FA	34.38	36.28 [6.7%]	33.47 [-2.6%]
FA (no rudders)	33.41	34.96 [5.9%]	32.40 [-3.0%]
FA (no appendages)	28.72	28.23 [-2.6%]	26.96 [-6.1%]

The appended drag contributions from the rudders or from the entire appendage suite can be calculated by subtracting the resistances in the third and fourth rows from the second row in Table 6. The difference and deviation percentage are shown in Table 7. The total resistance for the fully appended configurations remains unchanged from Table 6. The rudder drag and appendage drag are divided by the resistance from the fully appended configuration in each column. As an example, the measured data are shown in the second column where the rudder contributes 2.82% of the total drag and the appendage suite contributes 16.46% of the total drag. In the third column the CFD result with the *k-ε* Rt model predicted 3.64% from rudders and 22.19% from appendages. The last column shows the realizable *k-ε* model predicted 3.20% of the total resistance from rudders and 19.45% from the appendages. Based on the previous discussion, we found that the realizable *k-ε* model shows better prediction than the *k-ε* Rt model in the current appendage drag calculation.

Table 7 Comparison of appendage drag with measured data and CFD predictions

description	Fx (measured) lbf	Fx (Computation) lbf	Fx (Computation) lbf
	[Deviation (%)]	[Deviation (%)]	[Deviation (%)]
		<i>k-ε</i> Rt	Realizable <i>k-ε</i>
FA	34.38	36.28	33.47
FA (no rudders)	-0.97 [2.82%]	-1.32 [3.64%]	-1.07 [3.20%]
FA (no appendages)	-5.66 [16.46%]	-8.05 [22.19%]	-6.51 [19.45%]

## The Effect of Propeller Hub and Fairwater

The shaft geometry for all the previous analysis involves only the cut off shaft after the second pod which matches the shaft geometry in the model test. However, in reality the full scale geometry should always include a propeller, hub and fairwater. Therefore, the CFD prediction could be more accurate if the detailed geometry were included in the model. The geometries of the shaft with fairwater and the shaft without fairwater are shown in Figure 6. The shaft in the foreground shows the propeller hub, fairwater and a transition segment between the shaft pod and the propeller hub. The shaft in the far field shows a cut off after the second shaft pod. Note that the configuration shown in Figure 6 is for illustration purposes only because there is no configuration with mismatched geometry at the end of the propeller shafts in the CFD models. The configuration with propeller hub and its fairwater will be analyzed in the following sections.

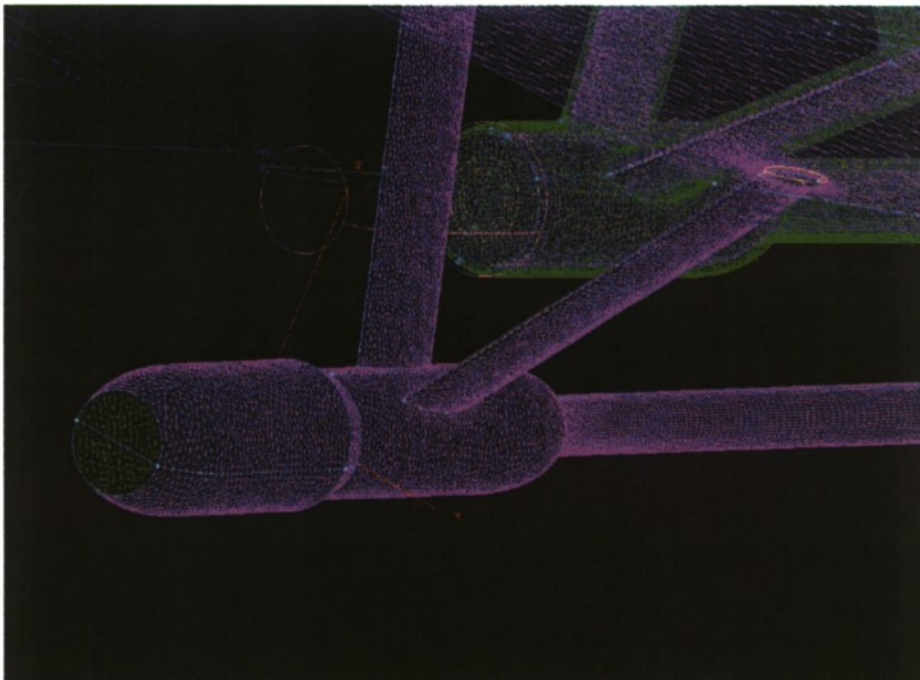


Fig. 6 Comparison of surface grid on the appendages with and without propeller extension hub fairwater

The total appended drag contributions from these two geometries can be broken down into rudders; the inboard shaft and struts; and the outboard shaft and struts. Each group in column 1 of Table 8 represents the sum of the elements on both port and starboard. The fifth row shows the total appendage drag from the breakdown and the last row shows the total drag of the fully appended configuration. First of all, the appendage drag, the sum of resistance of rudders, struts and shafts, for the case without propeller hub and the fairwater is 6.583 pounds which is about 19.66 percent of the total drag, 33.47 pounds. In comparison, the appendage drag for the case with propeller hub and the fairwater is 6.064 pounds which is about 18.39 percent of its total drag, 32.96 pounds. By comparing the total drags in the second and the third columns, there is 0.519 pounds drag reduction by adding the hub and the fairwater in the CFD model which is about 1.55% based on 33.47 pounds.

Table 8 Resistance contribution from the appendages

Appendage Elements	Drag (lbf) / Contribution	Drag (lbf) / Contribution	Drag (lbf) / Contribution
	$k$ - $\epsilon$ (no fairwater)	$k$ - $\epsilon$ (with fairwater)	$k$ - $\epsilon$ (with fairwater)
	CFD++ [base on 33.47]	CFD++ [base on 32.96]	CFD++ [base on 33.47]
Rudder	1.467 [ 4.38%]	1.510 [4.58%]	[4.51%]
S&S (inboard)	2.625 [ 7.84%]	2.356 [7.148%]	[7.04%]
S&S (outboard)	2.491 [ 7.44%]	2.198 [6.668%]	[6.56%]
Appendages Drag	6.583 [19.66%]	6.064 [18.39%]	[18.11%]
Hull	20.27 [60.65%]	20.83 [63.21%]	[63.78]
Total Drag	33.47	32.96	

Noticeably, the drag from the rudders shows a slight increase in the case with propeller hub and fairwater, 4.58%, compared to the case without hub and fairwater, 4.38%. The resistance increase on the rudder may be due to the interaction between the extended fairwater and the rudders.

Similarly, the drag from both inboard and outboard shafts and struts for the case with propeller hub and fairwater are significantly reduced compared to the case without propeller hub and fairwater. The pressure contours on solid walls are shown in Figure 7 and the separation regions, the iso-surface of the reverse axial velocity  $u$ , at the end of propeller shaft and at the junctures of appendages are indicated in blue. In comparison, the separation at the blunt base of the cut off shaft on the right of Figure 7 is stronger than the shaft with fairwater (left of Figure 7), which allows quicker pressure recovery and increase in the base pressure.

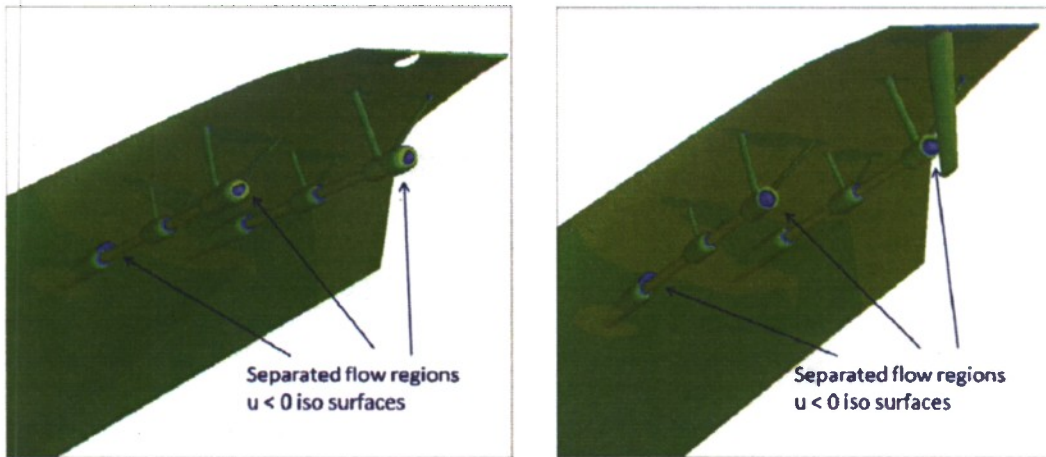


Fig. 7 Comparison of pressure contours and the flow separation on the appendages with propeller extension hub fairwater (left) and without propeller extension hub fairwater (right)

To explain the phenomena, the pressure contours on the rudders and appendages of these two configurations are compared in Figure 8 and the close up view for this comparison is shown in Figure 9. On the left figure of Figure 9 the pressure at the end of the propeller hub fairwater shows higher pressure than the pressure at the rear end of the shaft shown on the right of Figure 9. The higher pressure at the end of the fairwater may have contributed to the drag reduction on the propeller shaft shown in Table 9. However, this pressure rise may also increase the pressure at the leading edge of the rudder and subsequently increases the drag on the rudders. As a result, it appears that the reduction of resistance on the shaft is more significant than the resistance increase on the rudders because the total resistance for the geometry with propeller hub and fairwater is less than the total resistance from the geometry with cut off shaft.

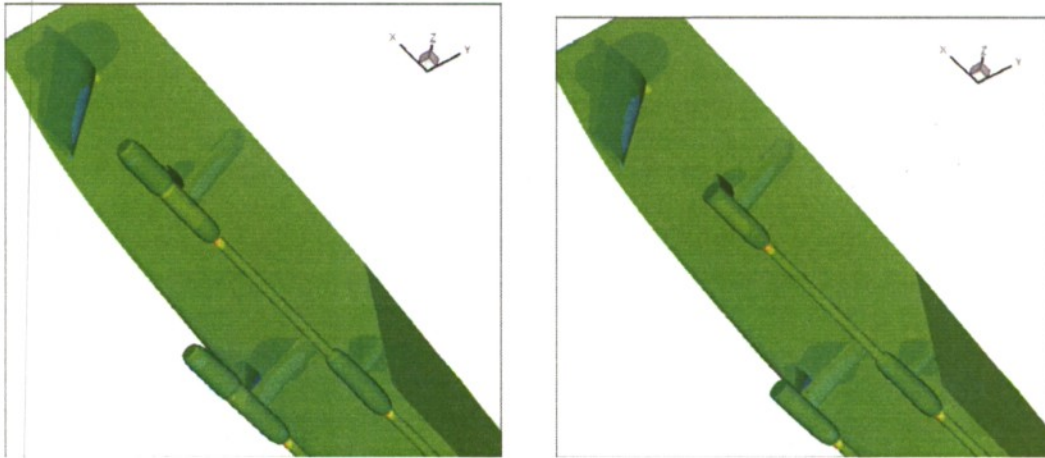


Fig. 8 Comparison of pressure contours on the appendages with propeller extension hub fairwater (left) and without propeller extension hub fairwater (right)

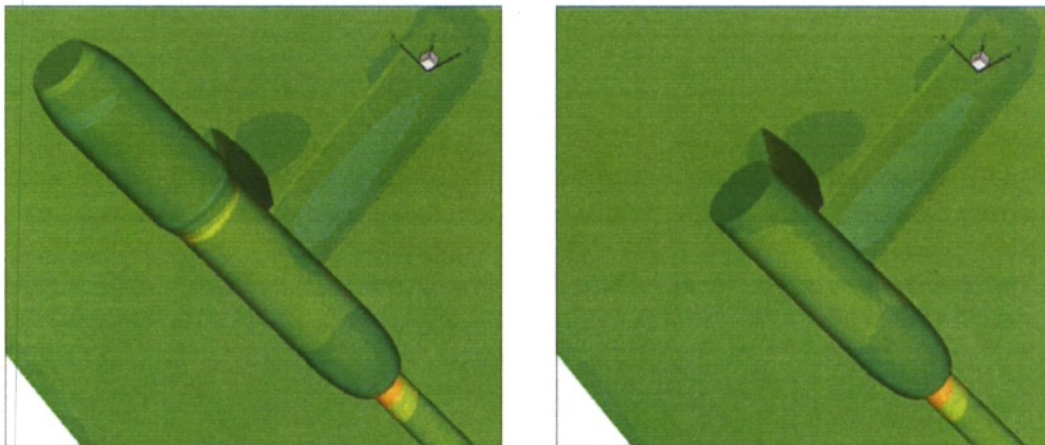


Fig. 9 Comparison of pressure contours on the appendages with propeller extension hub fairwater (left) and without propeller extension hub fairwater (right) (close up view)

The appended drag contribution can also be compared based on the bare hull resistance in Table 9. The measured bare hull resistance is 28.72 pounds and the measured resistance for the fully appended configuration is 34.38 pounds. The resistance increment based on the measured bare hull resistance is 5.66 pounds which is about 19.71%. In comparison, the CFD prediction using the realizable  $k-\epsilon$  turbulence model can predict the total drag very well. For the case without propeller hub and fairwater, the predicted total resistance for the fully appended configuration is 33.47 pounds resulting in 6.5 pounds over the measured bare hull resistance. The ratio of the appendage resistance with respect to the bare hull resistance is 22.63% and it is about 2.92% over predicted than the measured data in column 2. Similarly, the CFD prediction using the realizable  $k-\epsilon$  turbulence model shows 32.96 pounds for the fully appended configuration. The predicted appendage resistance is 5.99 pounds which leads to a 20.86% contribution with respect to the measured bare hull resistance. The deviation from the measure appendage resistance is about 1.15%.

Table 9 Resistance contributions from the appendages

Total Drag Fx	Measured (lbf)	CFD Realizable $k-\epsilon$ (no fairwater)	CFD Realizable $k-\epsilon$ (with fairwater)
Bare Hull only	28.72		
FA (fully appended)	34.38	33.47	32.96
dFx	5.66	6.5	5.99
dFx/Hull percentage based on exp.	19.71%	22.63%	20.86%
Deviation	0	2.92%	1.15%

### The Detailed Break Down of Drag Contribution from Each Element

The drag contributions from each element of the shafts and struts are listed in Table 10. This break down table is based on the fully appended result with propeller hub and fairwater using the realizable  $k-\epsilon$  turbulent model. The drag in the list is for a single element only such that the total appendage drag in each column of Table 10 is half of the total appendage drag in the third column in Table 8 accordingly. A list of all the appendage elements is shown in Figure 10. In general, the geometries for the inner shaft set and the outer shaft set are very similar except the first shaft pod, where the inner shaft pod is longer than the outer shaft pod.

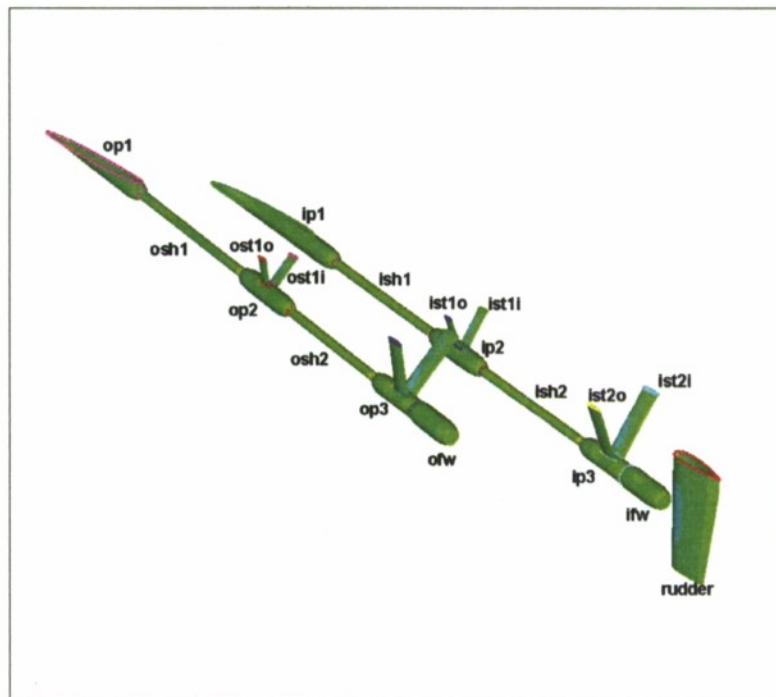


Fig. 10 Appendage elements of inboard and outboard sets

The nomenclature of the elements in the table are listed as follows and the outboard is arranged in the same manner but started with 'o' instead of 'i':

ip1	inboard shaft pod #1	op1	outboard shaft pod #1
ip2	inboard shaft pod #2	op2	outboard shaft pod #2
ip3	inboard shaft pod #3	op3	outboard shaft pod #3
ish1	inboard shaft segment #1	osh1	outboard shaft segment #1
ish2	inboard shaft segment #2	osh2	outboard shaft segment #2
ist1i	inboard strut set #1, inner element	ost1i	outboard strut set #1, inner element
ist1o	inboard strut set #1 outer element	ost1o	outboard strut set #1 outer element
ist2i	inboard strut set #2, inner element	ost2i	outboard strut set #2, inner element
ist2o	inboard strut set #2, outer element	ost2o	outboard strut set #2, outer element
ifw	inboard fairwater	ofw	outboard fairwater

The drag contribution from each appendage element is listed in Table 10, where the elements from the inboard shaft set are listed in the left two columns and the elements of the outboard shaft set are listed in the right two columns. With one on one comparison, several elements in the inboard shaft set behave similarly to the outboard shaft set, where the items highlighted in bold show very similar contributions to the total appendage drag. For example, drag contributions of the inboard item and the outboard item from the shaft pod #2, shaft #2, strut set #1, and strut set #2, are equal or differ by less than 5%.

Some elements show significant difference between the inboard and outboard. For example, for shaft pod #1, the inner one is about 4% larger than the outboard one, due to the difference in length. Some differences between correspondent elements do not have clear explanations, for example, the shaft pod #3, the shaft segment #1 and the strut set #2.

The significant differences in drag from the inner fairwater and the outer fairwater are most likely due to the interaction between elements. The fairwater of the inboard shaft set is very close to the rudder and the fairwater of the outboard shaft set is clear from other elements. The interaction between the fairwater and rudder increases the pressure on both the fairwater and the leading edge of the rudder, shown in Figure 10. Therefore, the resistance of the inboard fairwater is less than the outboard fairwater.

Table 10 RANS calculation for the appendage resistance study

Appendage element (inboard)	Drag (lbf)	Appendage element (outboard)	Drag (lbf)
ip1 (shaft pod #1)	0.149	op1 (shaft pod #1)	0.145
ip2 (shaft pod #2)	<b>0.158</b>	op2 (shaft pod #2)	<b>0.159</b>
ip3 (shaft pod #3)	0.186	op3 (shaft pod #3)	0.173
ish1 (shaft #1)	0.067	osh1 (shaft #1)	0.095
ish2 (shaft #2)	<b>0.081</b>	osh2 (shaft #2)	<b>0.080</b>
ist1i (strut set #1 inner)	<b>0.049</b>	ost1i (strut set #1 inner)	<b>0.049</b>
ist1o (strut set #1 outer)	<b>0.038</b>	ost1o (strut set #1 outer)	<b>0.036</b>
ist2i (strut set #2 inner)	0.175	ost2i (strut set #2 inner)	0.151
ist2o (strut set #2 outer)	<b>0.144</b>	ost2o (strut set #2 outer)	<b>0.137</b>
ifw (fairwater)	0.049	ofw (fairwater)	0.151
Total inboard appendage drag	1.099	Total outboard appendage drag	1.178

A close up view of the fairwaters in Figure 11 shows lower pressure at the outboard fairwater than the pressure on the inboard fairwater. This pressure difference may explain why the drag acting on the inboard fairwater is lower than the drag acting on the outboard fairwater.

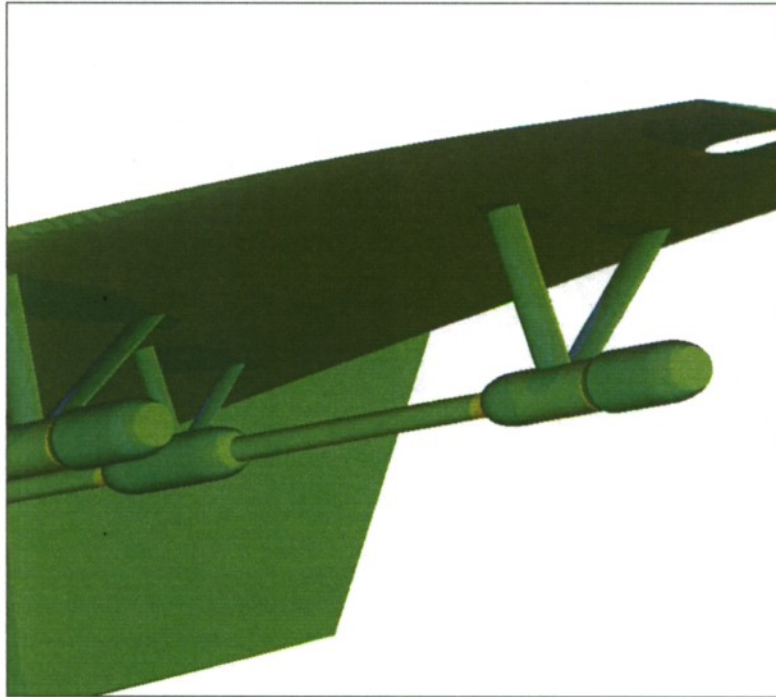


Fig. 11 Pressure contours on the inboard and outboard fairwaters

## Conclusions

The following are concluded for numerical prediction using CFD++ for the JHSS appendage resistance.

1. In general, the RANS solver CFD++ provides very reasonable predictions compared to the model test data.
2. The  $k-\varepsilon$  Rt turbulence model predicts higher resistance than the realizable  $k-\varepsilon$  turbulence model, which provides predictions closer to the measured data. It should be noted that the free surface was not included in this analysis. Therefore, the low drag predictions for the  $k-\varepsilon$  model are arguably more reasonable.
3. The model with propeller hub and fairwater predicts less resistance than the model with cut off shaft pod. The gradual curvature from the propeller hub to the fairwater prevents massive flow separation from the propeller hub, which then improves pressure recovery, and significantly reduces total resistance.
4. The resistance reduction from adding the propeller hub and the fairwater should be considered in future model tests and CFD analysis for better performance.

THIS PAGE INTENTIONALLY LEFT BLANK

## References

1. EmPower, "Empirical Power Prediction program", developed by MARINTEK, Norway.
2. HOLTROP, "A Statistical power prediction program", based on Holtrop, J. and Mennen, G.G. J., "An Approximate Power Prediction Method", International Shipbuilding Progress, Vol.29, No. 335, July 1982.
3. SHIPFLOW, "Virtual Towing Tank CFD Prediction Power", Denmark.
4. Hullspeed, "A Resistance Prediction Program – a Regression Based Method", Formation Design Systems Pty Ltd.
5. Lasky, M. P., "An Investigation of Appendage Drag", NSRDC Report 458-H-01, March 1972.
6. Kirkman, K. L., Sanders, D. G. and Slager, J. J., "Methodology for Computation of Appendage Resistance", HYDRONAUTICS, Incorporated Tech Report 7809.33-1, October 1979.
7. Liu, H. L., "EXCEL Spreadsheets for Appendage Drag Evaluation – Shaft/Strut and Pod", NSWCCD-50-TR-2007/074, September 2007.
8. Cusanelli, D. S., "Joint High Speed Sealift (JHSS) Baseline Shaft & Strut (Model 5653) Series 1: Bare Hull Resistance, Appended Resistance, and Alternative Bow Evaluations", NSWCCD-50-TR-2006-064, 2006.
9. Shih, T. H., Liou, W. W., Shabbir, A., and Zhu, J., "A New k-e Eddy-Viscosity Model for High Reynolds Number Turbulent Flow-Model Development and Validation", Computer Fluids, 24(3):227-238, 1995.
10. Aroussi, A., Kueukoglan, S., Pickering, S., and Menace, M. "Evaluation of Four Turbulence Models in the Interaction of Multi Burners Swirling Flows", 4<sup>th</sup> International Conference on Multiphases Flow, New Orleans, LA, June 2001.
11. Goldberg, U. C., "Exploring a three-equation R-k-e turbulence model", ASME J. Fluids Engrg. 118 796, 1996.
12. Goldberg, U., Peroomian, O., and Chakravarthy, S., "Application of the k-e-R Turbulence Model to Wall-Bounded Compressive Flows", AIAA 98-0323, 1998.

THIS PAGE INTENTIONALLY LEFT BLANK

### Initial Distribution

Print	Center Distribution					
	Code	Name	Print	PDF	Code	Name
1	NAVSEA 05		1		3452	Library
1	05	Webster	1		5060	Walden
1		DTIC		1	5500	Griggs
				1	5500	Drezin
				1	5700	Jiang
			2		5800	File
				1	5800	Black
			1		5800	